Dynamic RCS Estimation of Chaff Clouds

DONG WOOK SEO
HYUN-JAE NAM
OH-JOON KWON
NOH HOON MYUNG, Member, IEEE
KAIST

We analytically investigated electromagnetic wave propagation through chaff clouds. The chaff fibers are assumed to be long and thin cylinders. The trajectory tracking algorithm was developed based on a combination of the six degree-of-freedom (6 DOF) equations of motion and the aerodynamic forces and moment acting on the chaff fibers. For the low Reynolds number flows around the chaff fibers, the normal force was obtained from a curve-fit formula offered by Sucker and Brauer, while an analytic solution offered by Curle is used to obtain the tangential force. The position and orientation of the chaff fibers as a function of time are thereupon obtained. As inputs of a generalized equivalent conductivity (GEC) method, this information is used to calculate the radar cross section (RCS) of the chaff cloud. The GEC method can estimate the RCS of a chaff cloud with an arbitrary orientation distribution for reducing computation time. The proposed chaff cloud model (CCM) can be applied to predict accurately the steady state response as well as the transient response before the RCS of the chaff cloud reaches the steady state.

Authors' current addresses: D. W. Seo, Defense Agency for Technology and Quality, Daegu Center 1st team, 1369-2, Manchon 1-dong, Suseong-gu, Daegu, 706-803, Korea, E-mail: (seodongwook@kaist.ac.kr); H-J. Nam, O-J. Kwon, and N. H. Myung, Korea Advanced Institute of Science and Technology (KAIST), Daejon, Korea.

I. INTRODUCTION

Chaff is widely used in modern warfare to degrade the accuracy rate of guided weapons using radar sensors. It is composed of small and thin pieces of glass fibers plated with aluminum or silver and is dispersed in the air like a cloud from air fighters or warships. The chaff cloud is deceptively displayed as another target on the radar screen or disturbs the radar screen through multiple reflected signals. Since the chaff fibers are dispersed in the air, its orientation and position change with respect to time by the aerodynamic forces around the chaff fibers. Thus, the radar cross section (RCS) of the chaff cloud also changes with respect to time. To estimate the RCS of the chaff cloud, two parts are distinguished: the aerodynamics part to determine the orientation and position of chaff fibers using the aerodynamic model, and the RCS part to calculate the RCS of the chaff cloud with respect to time. The flow chart of Fig. 1 shows how the aerodynamics and the RCS of chaff clouds can be estimated.

Each chaff fiber has a long and thin cylindrical rod structure. The characteristics of cylindrical rods with a high aspect ratio have been studied for decades [1–3]. There also is a large body of experimental research on multiple chaff fibers and chaff cloud dynamics [4–7]. According to the findings of previous studies, the falling chaff has remarkable characteristics, that is, the falling speed is less than one m/s and it falls with horizontal orientation. Recently, some literatures have studied the chaff cloud models (CCMs) [8–13]. Xianli [8] and Jian-chun [9] established mathematical models of chaff cloud jamming RCS. These CCMs are based on time-unvarying RCS and position. Ducata [10], Qu [11], and Wu [12] introduced chaff cloud motion models (CCMMs). The built CCMMs are used to design the major launch parameter such as the time spacing between launching every chaff cartridge and the number of chaff cartridges [12]. However, important time parameters used in these CCMMs such as the effective time of duration are not determined by aerodynamics but set by empirical results. In [13] the results of aerodynamics such as the distribution and orientation of chaff fibers were obtained by a CCM under the assumption that the orientation and angular speed of the chaff fibers are known in the steady state. Since this approach used a constant orientation distribution and angular speed, accurate estimation from an initial launch having an arbitrary orientation to the steady state cannot be accomplished. In addition, if the features of the chaff fibers such as aspect ratio and mass vary slightly, new information about the orientation and angular speed of the chaff fibers should be obtained through experiments. To overcome these drawbacks and to provide an accurate prediction of the orientation and position of chaff fibers dispersed with an arbitrary orientation, we
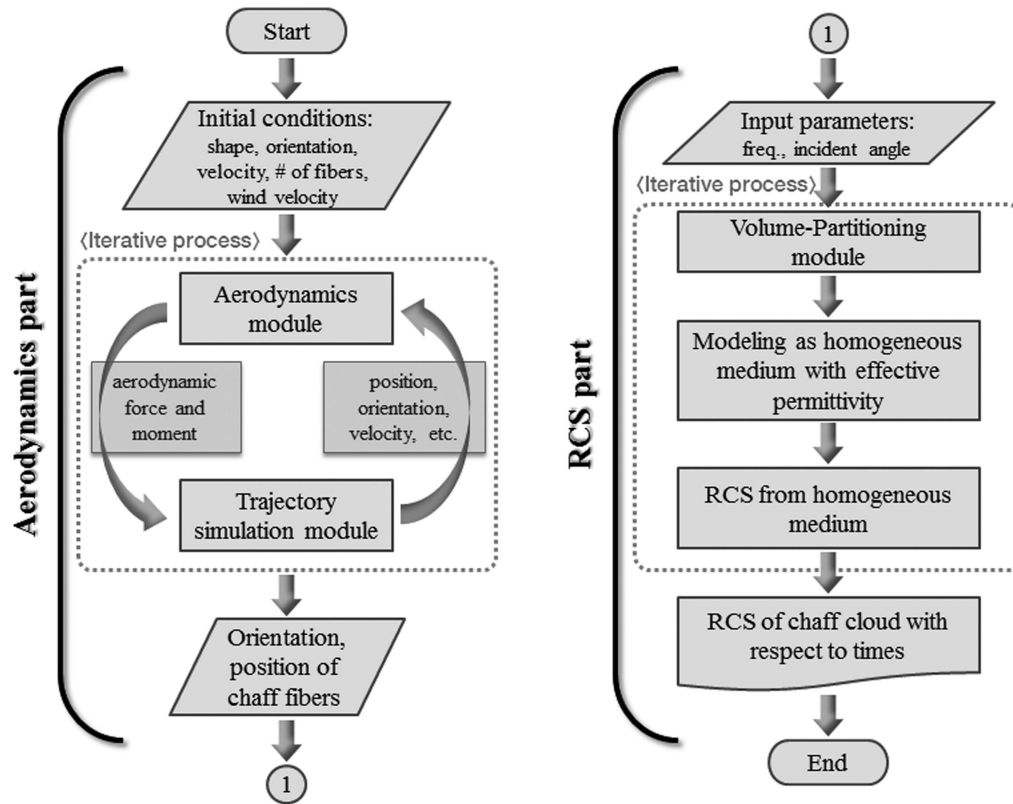
Fig. 1. Flow chart for estimating aerodynamics and RCS of chaff clouds with respect to times.

propose a trajectory tracking algorithm based on a combination of six degree-of-freedom (6 DOF) equations of motion and the aerodynamic forces.

For analysis of the RCS of a chaff cloud, studies on the RCS of wire scatterers can be used [14–19]. However, the number of chaff fibers within a chaff cloud is extremely large. Therefore, numerical methods requiring accurate orientation and position of all scatterers such as the method of moment (MoM) [14] and finite-difference time-domain (FDTD) [15] cannot, in practice, calculate the RCS of the chaff cloud due to excessive computing time and limited memory capacity. In [20], the iterative MoM and multilevel fast multipole method (MLFMM) solver of a commercial EM tool are used to calculate the RCS of about two thousand chaff fibers, but still those need a lot of computer resource and memory.

For these reasons, the RCS of a chaff cloud is simply expressed as the multiplication of the average RCS of a single chaff fiber and the total number of chaff fibers in most cases [21, 22]. However, this approach is valid only when the distance between each fiber is larger than 2λ so as to ignore the effect of mutual coupling. That is, this approach cannot be used for the initial launch of chaff where chaff fibers are gathered. The normalized RCS density presented in [13] also does not consider mutual coupling between chaff fibers, and simply combines the average RCS and the density of chaff fibers. Therefore, the normalized RCS density is not a quantity related to

the RCS, but rather only gives the density of fibers with horizontal orientation and vertical orientation. On the other hand, the recently introduced generalized equivalent conductor (GEC) method considers wire scatterers with an arbitrary orientation distribution as a homogeneous medium and calculates the RCS from this homogeneous medium [23]. Therefore, this approach enables fast computation for the RCS of the chaff cloud.

Despite the abundance of methods developed to estimate the RCS of wire scatterers, there have been few studies on variation of the RCS of an actual chaff cloud with respect to time. In this paper, a chaff cloud with an extremely large number of chaff fibers is divided into sub-blocks that depend on the density of chaff fibers, and the RCS of each sub-block is quickly calculated by using the GEC method. Finally, the total RCS of the chaff cloud is calculated as the sum of the RCSs of sub-blocks. Therefore, we can accurately estimate the RCS of the chaff cloud from the initial launch to the steady state.

According to the sequence of the flow chart of Fig. 1, this paper is organized as follows. In Section II the aerodynamic forces of chaff fibers in the direction of the fiber length and perpendicular to the fiber length and the overall procedure of the trajectory tracking algorithm are briefly explained. The unique chaff fiber characteristics according to the initial conditions are described by using the trajectory tracking algorithm in Section III. In
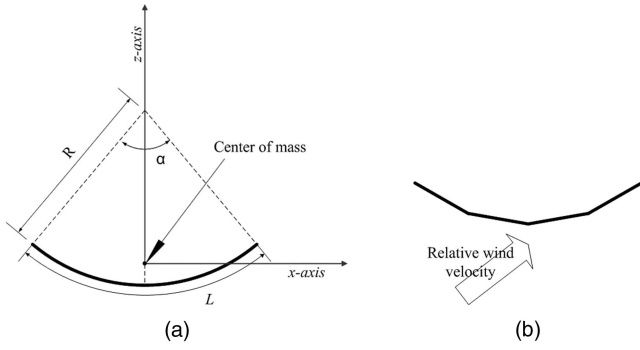
Fig. 2. Geometry of single chaff fiber. (a) Typical chaff of longitudinal bent fiber. (b) Modeling of longitudinal bent fiber with several straight sections.

Section IV the proposed approach to calculate the RCS of extremely numerous scatterers is presented. In Section V the results of the RCS for a falling chaff cloud with respect to time are shown by using the orientation and position of the chaff cloud based on the trajectory tracking algorithm. Finally, Section VI draws conclusions and provides a summary of this work.

II. AERODYNAMIC MODEL OF CHAFF

In the present study, a numerical methodology for simulating the trajectory of chaff fibers is developed. The methodology consists of two modules: one for aerodynamic loads calculation, and the other for the trajectory simulation by 6 DOF equations of motion. In Subsection A, a description of the aerodynamic loads calculation is presented, and determination of the chaff position and orientation in time coupled with the 6 DOF equations of motion is explained in Subsection B.

A. Aerodynamics Module

The configuration of the chaff fibers is generally assumed to be a slender circular cylinder with a uniform cross section. The chaff fibers have a high aspect ratio with length L and very small cross section diameter D. The typical diameter of the chaff fibers is about 2×10^{-5} m, which corresponds to a Reynolds number of unity. The Reynolds number is defined as the ratio of the inertia force to the viscous force, and thus at this low Reynolds number the viscous force is much greater than the inertia force of the fluid. As a result, the aerodynamic damping moment which affects the inclination of the elevation angle tends to be large. Chaff fibers are normally straight, however, in real operation situations the fibers may have longitudinal bending [24]. Thus, it is assumed that the chaff configuration of a longitudinally curved fiber has the shape of a circular arc with longitudinally bent radius R and its corresponding central angle α. The typical shape of a deformed fiber with longitudinal bend is shown schematically in Fig. 2(a).

Chaff fiber as a rigid body performs free translational and rotational motions under the influence of gravity and the aerodynamic force and moment caused by its own motions. To estimate these aerodynamic loads effectively, each chaff fiber is assumed to consist of several straight sections as shown in Fig. 2(b). The relative wind velocity due to these motions is decomposed into normal and tangential components to each section. Then, the normal and tangential forces at each section are obtained from the decomposed wind velocity, and the total force on the chaff fiber is obtained by the sum of the forces acting on each section. The total aerodynamic moment is also obtained in a similar way by adding the contribution from each section with respect to the center of mass of each chaff fiber.

To obtain the normal force, a curve-fit formula of the experimental data for the drag of a circular cylinder in crossflow at very low Reynolds numbers offered by Sucker and Brauer [1] was used. An analytical solution by Curle [2] based on the boundary layer theory was used to evaluate the axial force. The solution was obtained for the axisymmetric laminar boundary layer in axial flow along a long thin circular cylinder by expanding in powers of the ratio of the boundary layer thickness to the cylinder radius. The resulting force coefficients at Reynolds numbers between 0 and 2 are shown in Fig. 3. The figure shows that the forces are in good agreement with the experimental data for the given geometry [3]. As shown in the figure, the normal force is approximately eight times larger than the axial force in the case of a fiber with $D = 2.54 \times 10^{-5}$ m and $L = 2.54 \times 10^{-2}$ m. This means that the normal force is a predominant factor which affects the flight behavior of a fiber, compared with the axial force.

B. Trajectory Simulation Module

From the aerodynamics module, the aerodynamic force and moment on each chaff fiber are obtained in the xyz body-fixed coordinate system with its origin at the center of mass of the fiber as shown in Fig. 2(a). The translational and rotational motion of a fiber in three-dimensional space has 6 DOF, and can be described by the six nonlinear differential equations [25]:

$$
\begin{aligned}
\sum F_x &= m(\dot{U} + QW - PV) \\
\sum F_y &= m(\dot{V} + RU - PW) \\
\sum F_z &= m(\dot{W} + PV - QU) \\
\sum L &= \dot{P}I_x + QR(I_z - I_y) + I_{xy}(PR - \dot{Q}) \\
\sum M &= \dot{Q}I_y + PR(I_x - I_z) - I_{xy}(QR + \dot{P}) \\
\sum N &= \dot{R}I_z + PQ(I_y - I_x) + I_{xy}(Q^2 - R^2).
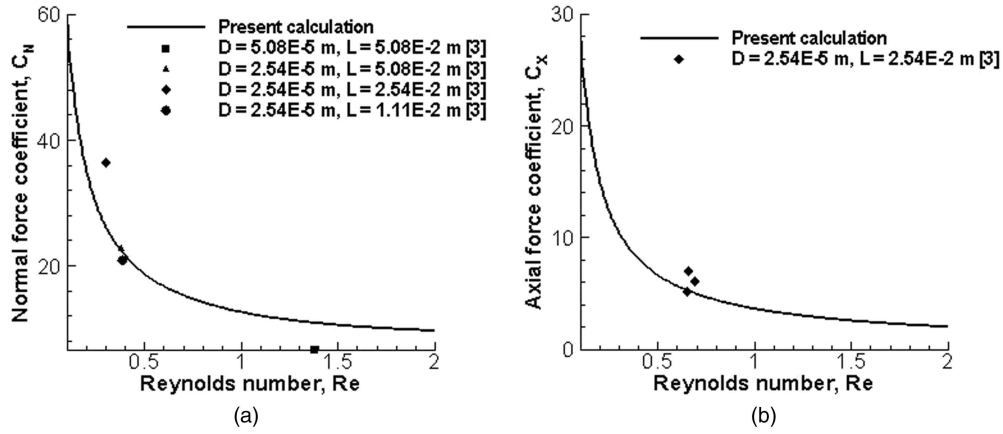\end{aligned}
\tag{1}
$$

Fig. 3. Correlation of force coefficients with Reynolds number. (a) Normal force coefficient. (b) Axial force coefficient.
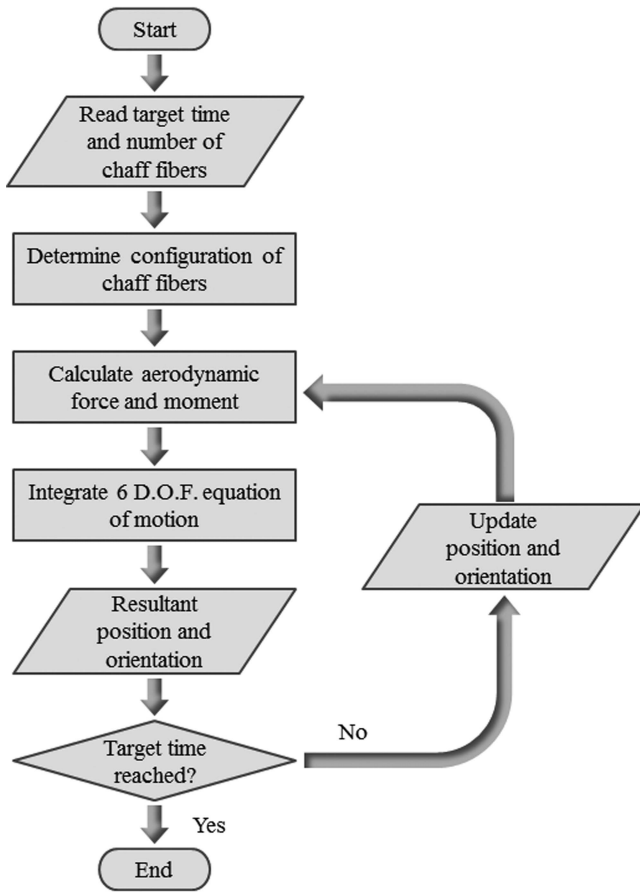

Fig. 4. Iterative procedure for trajectory tracking algorithm.

Here F_x, F_y, and F_z are the force components, and L, M, and N are the aerodynamic moments in the xyz body-fixed coordinate system. U, V, and W are the velocity components, and P, Q, and R are the angular velocity components, respectively. Also, I is the moment-of-inertia of the fiber and m is the mass of the fiber. Once the position and the orientation of the fiber are obtained, they can be transformed into the XYZ inertial coordinate system by introducing the Euler angle. The X- and Z-axis denote the horizontal distance and the height,

respectively, and the X-Y plane denotes the plane parallel to the ground. The absolute velocities are also obtained in terms of the Euler angles and the velocity components from the body-fixed frame. The Euler rates are obtained in terms of the angular velocities in the body-fixed frame. By integrating the velocities and the Euler rates, the position and the orientation of each fiber are determined at the current time step, and the information is provided as the input values to the aerodynamics module for the next time step.

The outline of the overall procedure for the trajectory tracking algorithm is presented in Fig. 4. For the given values of target time and number of chaff fibers, the configurational properties of the chaff fibers are determined. From the known translational and rotational motion relative to the position and the orientation of the chaff fiber, the aerodynamic force and moment are calculated. These three components of aerodynamic force and moment are provided as the input values to integrate the 6 DOF equations of motion in (1) for the next time level and to obtain the velocities and the Euler rates of each chaff fiber. By integrating these values, the new chaff position and orientation are determined at the next time step. For this time integration, the fourth-order accurate Runge-Kutta method is used [26]. The time step size was set to 2×10^{-3} s. These updated chaff position and orientation are provided to the aerodynamics module for the next time step. This fully coupled iterative process is repeated until the computed time reaches the target time.

III. CHARACTERISTICS OF DYNAMICS OF CHAFF

After the completion of the trajectory simulation, the flight characteristics of all chaff fibers are obtained. Among them, the position and the orientation of the chaff fibers are the most important two factors when the RCS is to be determined, including the effect of the geometric curvature of the chaff fibers.
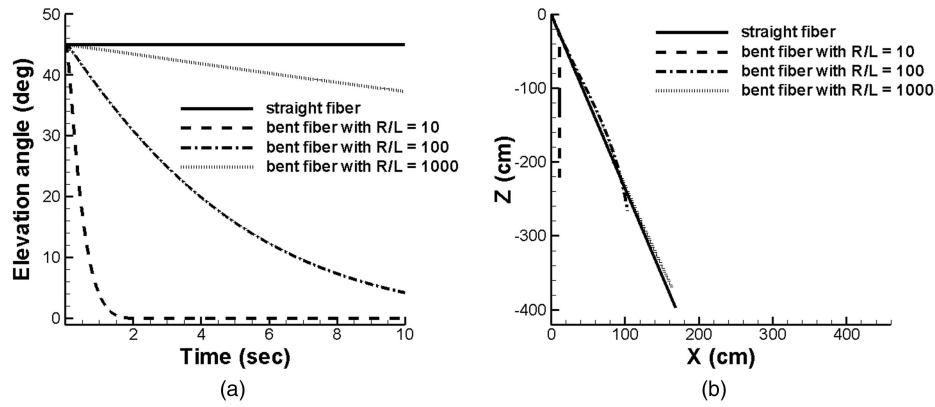
Fig. 5. Comparison of flight characteristic parameters between straight fiber and bent fibers. (a) Orientation history with time. (b) Position history in vertical plane (*X-Z* plane).

TABLE I
Configurational Properties of Chaff Fibers

Length (cm)	Diameter (μm)	Mass (μg)		Moments-of-Inertia ($g \cdot cm^2$)	
				I_{xx}	$I_{yy}(\times 10^{-6})$
1.78	28.42	27.2	straight fiber with $R/L = \infty$	2.7462×10^{-11}	7.1817
			bent fiber with $R/L = 1000$	1.1964×10^{-13}	7.1810
			bent fiber with $R/L = 100$	1.1963×10^{-11}	7.1810
			bent fiber with $R/L = 10$	1.1959×10^{-9}	7.1786

At first, the position and the orientation of each chaff fiber with time were calculated to examine the effect of geometric curvature on the flight behavior of the fibers. For this purpose, the radius of longitudinal bend is changed. The fiber with very large radius of longitudinal bend becomes a straight one. The ratio of longitudinal bend radius to chaff length is denoted as R/L. The configurational properties of the fibers tested are summarized in Table I. As shown in the table, the moments-of-inertia are slightly different between the straight fiber and the bent fibers with longitudinal bends of $R/L = 10$, except the moment-of-inertia along *x*-axis, I_{xx}.

One straight chaff fiber and the three fibers with different longitudinal bends were tested to examine the time history of the position and the orientation at the sea level atmospheric condition. The initial orientation of all four chaff fibers was assumed to be inclined at 45 deg with respect to the ground. The simulation was made for 10 s, and the results are presented in Fig. 5. As shown in Fig. 5(a), the straight fiber maintains its initial orientation during the free flight, while the orientations of the bent fibers tend to reduce the inclination and eventually become parallel to the ground. This phenomenon is qualitatively in good agreement with experimental data [4]. This means that in the case of a straight fiber, aerodynamic moment is not produced due to the geometric symmetry. On the other hand, in the case of the longitudinal bent fibers non-zero aerodynamic moment exists because the integrated resultant force

does not pass through the center of mass of the fiber. This aerodynamic moment applies in the direction to reduce the inclination, and eventually the orientation of the chaff fiber becomes horizontal. This angular motion in time is relevant to the magnitude of the radius of longitudinal bend, and the time to reach zero elevation angle is reduced as the longitudinal bend radius is smaller.

The results of the trajectory simulation in the vertical projection (*X-Z*) plane, normal to the ground, are presented in Fig. 5(b). As shown in the figure, the straight fiber travelled the largest horizontal distance of about 170 cm during 10 s, while the bent fiber with a longitudinal bend of $R/L = 10$ travelled the smallest horizontal distance. The flight behaviors of the bent fibers with larger longitudinal bends are similar to the straight one, and these phenomena coupled with the variation of the elevation angle of the fibers in time are shown in Fig. 5(a). As the elevation angle of bent fibers reaches zero, the chaff fiber travels only in the downward direction, and falls slower than others with a finite elevation angle.

Next, trajectory simulations of multiple chaff fibers were made to examine the dispersion pattern of chaff clouds. In general, an increased number of chaff fibers results in increasing the density of the chaff cloud in certain ranges. However, in the point of view of a dispersion pattern, an increment of the number of chaff fibers does not affect the dispersion pattern of the chaff cloud because the interaction between fibers is not the major concern. Thus, the number of chaff
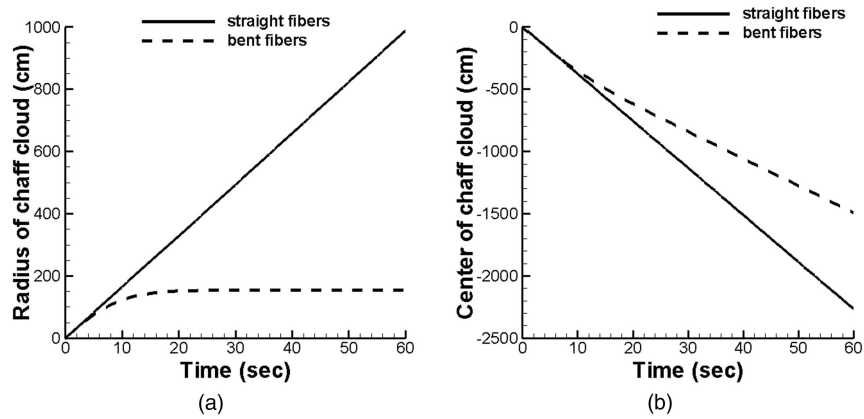
Fig. 6. Comparison of time histories of chaff cloud between straight fibers and bent fibers with R/L between 2 and 100. (a) Radius of chaff cloud. (b) Center of chaff cloud along Z-axis.
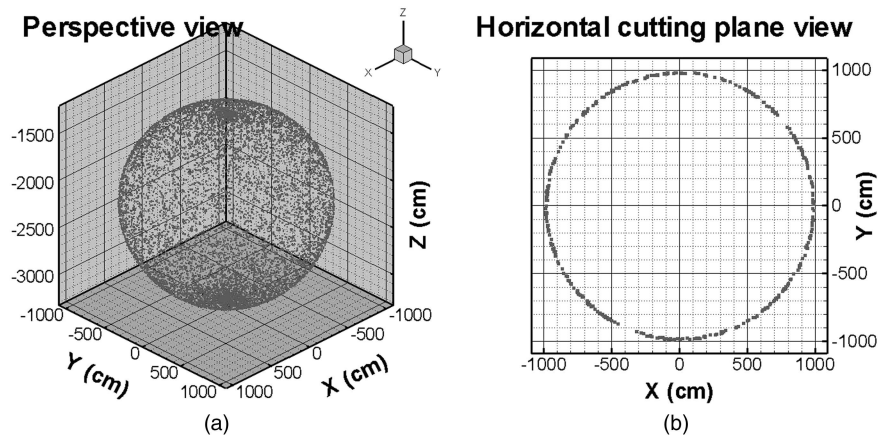

Fig. 7. Position distributions of straight fibers after 60 s. (a) Perspective view. (b) Horizontal X-Y cutting plane view.

fibers was set to 10,000. The fibers were assumed to be released from a fixed position in space (0,0,0) with randomly distributed orientations from 0 to 360 deg, and the simulation was made for 60 s. The trajectory simulations were performed with both the straight fibers and the bent fibers with longitudinal bends of R/L randomly generated between 2 and 100.

In Fig. 6 the time histories of the dispersion width and the vertical center of the chaff clouds are presented. The figure shows that the radius of the chaff cloud of straight fibers is linearly increasing as time increases, while that of the chaff cloud of the bent fibers stopped increasing after approximately 20 s. When the time reached 60 s, the radius of the chaff cloud of straight fibers is 1,000 cm, while that of the chaff cloud of fibers with the longitudinal bends is approximately 150 cm. Figure 6(b) illustrates that the cloud of straight fibers is falling faster than bent fibers. The descent rate of straight fibers is nearly constant with time, while that of bent fibers started to decelerate after about 10 s because most fibers are in steady state. After 60 s, the center of the chaff cloud of straight fibers approaches −2,300 cm, while that of the chaff cloud of fibers with longitudinal bends dropped −1,500 cm, approximately.

The position distributions of the straight fibers after 60 s are represented in Fig. 7. Dots represent the positions of straight fibers. It is shown that the chaff cloud of straight fibers forms a shell of a sphere shape and the positions of straight fibers are uniformly distributed on the shell. This is because the position of straight fibers is only characterized by their initial orientation. In Fig. 7(b), the distribution of straight fibers in a horizontal plane (X-Y plane) at the range between −2,400 and −2,300 cm is presented. The shape of the chaff cloud of straight fibers again shows a ring shape, confirming that the fibers are distributed in a circular pattern with a finite radius.

The position distributions of the bent fibers after 60 s are represented in Fig. 8. Dots represent the positions of bent fibers. The result shows that most fibers are located near the upper center of the chaff cloud, but the entire cloud forms a spheroid. This is because positions of the fibers are determined by both its initial orientation and the magnitude of the radius of longitudinal bend of each fiber. Thus the cloud of the fibers with various longitudinal bends does not form a regular pattern and its distribution is different from that of the straight fibers. Figure 8(b) shows the position distributions of bent fibers in a
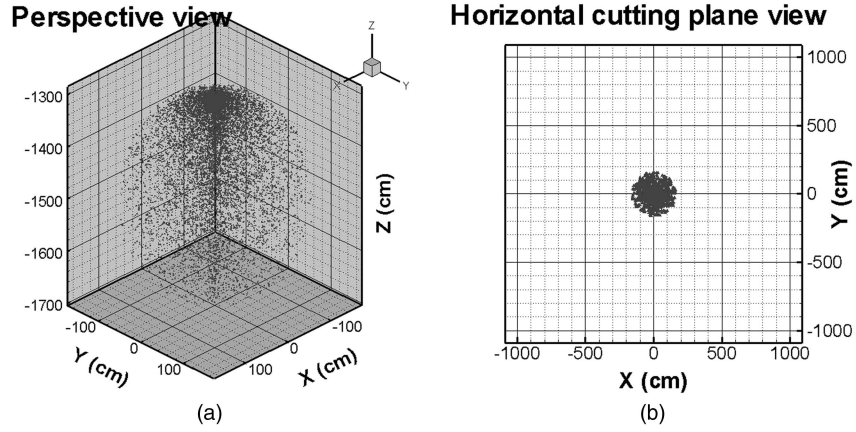
SEO, ET AL.: DYNAMIC RCS ESTIMATION OF CHAFF CLOUDS

2119

Perspective view

(a)

Horizontal cutting plane view

(b)

Fig. 8.   Position distributions of bent fibers after 60 s. (a) Perspective view. (b) Horizontal *X-Y* cutting plane view.
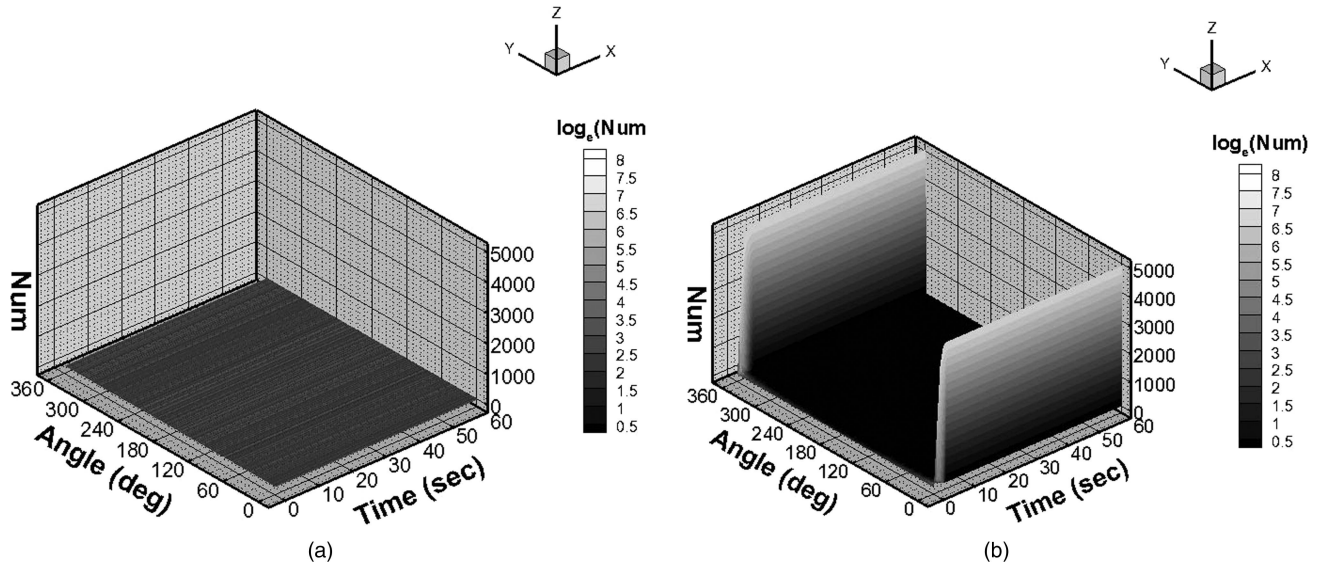

(a)

(b)

Fig. 9.   Time histories of orientation distributions. (a) Straight fibers. (b) Bent fibers.

horizontal cutting plane (*X-Y* plane) in the range of −1,500 to −1,450 cm along *Z*-axis. The slice of the chaff cloud of bent fibers shows a circle shape with the bent fibers with various radii of longitudinal bend, the position of the bent fibers can be affected by the magnitude of the radius of longitudinal bend. Thus, the fibers distributed inside the circle. The chaff fibers with small radius of longitudinal bend are positioned near the center of the cloud, and the fibers with large radius of longitudinal bend are placed further away from the center of the cloud. The size of the circle is relatively small compared with the one from straight fibers, as described in Fig. 6(a).

In Fig. 9 the time histories of the orientation distributions of the chaff fibers are represented. The contour level for the number of chaff fibers is drawn in a natural logarithm scale. It is shown that the orientation history of the straight fibers remains their initial orientation during the free flight, while the elevation angle of bent fibers tends to be reduced

in time, and the orientations become parallel to the ground within 10 s.

IV.   METHOD FOR CALCULATING THE RCS OF A CHAFF CLOUD

A.   Volume-Partitioning Procedure

The number of chaff fibers to form a chaff cloud generally reaches several million. As aforementioned, calculating the electromagnetic scattering of such a large number of scatterers at once is impossible due to the limitations of computer memory and calculation time. Therefore, in this paper, we consider the chaff cloud as a homogeneous medium with effective permittivity. However, by considering the chaff cloud as a single homogeneous medium, we oversimplify the problem. This is because the density and orientation of chaff fibers are not uniform throughout the cloud. We partition the volume of the chaff cloud into sub-blocks and calculate the total RCS of the chaff cloud as the sum of the RCSs of
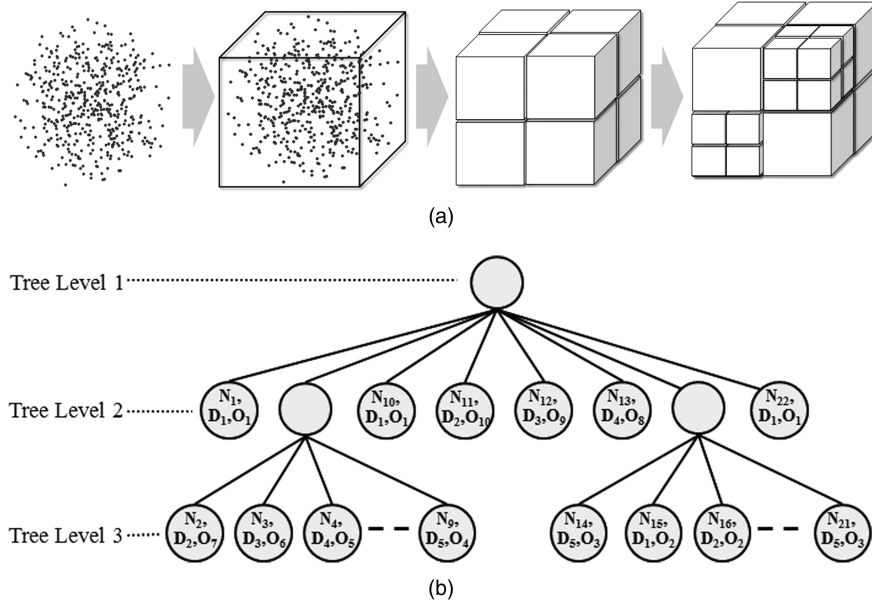
Fig. 10. (a) Recursive subdivision of chaff cloud into eight sub-blocks. (b) Tree structure of sub-blocks arranged by recursive subdivision.

all sub-blocks. As shown in Fig. 10(a), the chaff cloud is divided by the number of chaff fibers in the sub-block. In order to partition the volume of the chaff cloud, an octree algorithm is used. The octrees are most often used to partition a three-dimensional space by recursively subdividing it into eight regions. The termination condition of this recursive algorithm is that the number of chaff fibers is less than one thousand in each sub-block. Figure 10(b) presents sub-blocks created through the partition process as a tree data structure. In this figure, the maximum tree level is three, and N_1 through N_{22} written in each tree node is the number of chaff fibers within the corresponding sub-block; D_1 through D_{10} are the density levels, which are given depending on the density of each sub-block; and O_1 through O_{10} are the oriented distribution levels, which are given depending on the standard deviation of the zenith angle of chaff fibers.

As seen in the results of Section III and [13], chaff fibers do not distribute uniformly thorough the chaff cloud. That is, the local density of chaff fibers varies depending on the location within the chaff cloud. Therefore, the density level is determined by the average density of each sub-block. Orientation of chaff fibers also may not distribute uniformly. In particular, the distribution of the zenith angle of chaff fibers is an important factor affecting the RCS of the fibers. If the chaff fibers have a uniformly random orientation for all directions, the standard deviation of the zenith angle is 39 deg. Thus, the orientation level, divided into 10 sections between 39 deg and 0 degree, is given by the standard deviation of the zenith angle of the chaff fibers within a sub-block. Consequently, each sub-block is characterized by the tree level, the number of chaff fibers, density level, and orientated distribution level.

In order to reduce the time for calculation of total RCS of the chaff cloud, the precomputed RCS with the same tree level, density level, and orientation level is reused for the other sub-blocks. For example, in Fig. 10(b), if the RCS σ_1 of the 1st sub-block with $N1$ fibers, density level D_1, and orientation level O_1 is obtained, then the RCS of the 10th and 22nd sub-blocks with the same tree level, density level, and orientation level can be calculated as

$$\sigma_{10(\text{or } 22)} \approx N_{10(\text{or } 22)} \times \frac{\sigma_1}{N_1}. \tag{2}$$

Under the assumption that the mutual coupling among sub-blocks is negligible, the total RCS of the chaff cloud is obtained by the sum of the RCSs of all sub-blocks as follows:

$$\sigma_{\text{total}} \approx \sum_{i=1}^{M} \sigma_i \tag{3}$$

where M is the number of sub-blocks.

B. Calculation Method for the RCSs of Sub-Blocks

We should know the RCS of each sub-block for calculating the total RCS of the chaff cloud. The chaff cloud is a random media in which the chaff fibers have a random distribution. Numerical methods such as the MoM and the FDTD require an additional procedure such as a Monte Carlo simulation for application to random media. Conventionally, the problem of electromagnetic scattering in random media has been investigated using the radiative transfer method and the multiple scattering theory [27]. However, if a random medium consisting of
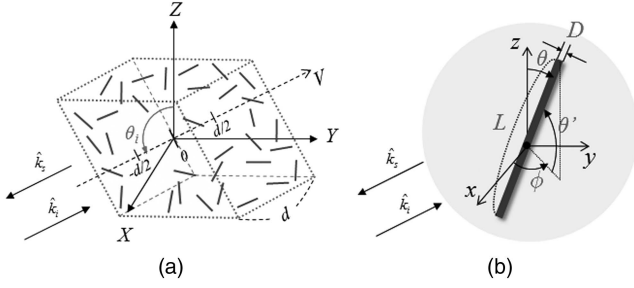
Fig. 11. Geometry of chaff fiber and sub-block of chaff cloud
for estimating RCS of sub-block. (a) Local coordinate of
sub-block with N chaff fibers by incident angle. (b) Orientation
and legnth of a single chaff fiber.

particles and a background medium is considered as
a homogeneous medium with an effective permittivity,
then estimating the electromagnetic scattering of the
random medium is very straightforward.

The recently introduced GEC method considers
wire scatterers with an arbitrary orientation
distribution as a homogeneous medium and calculates
the RCS from the homogeneous medium [23]. From
the results of Section III and measurements [5, 6],
it shown that actual chaff fibers fall horizontally
in the air. Thus, the GEC method can reflect the
actual orientation of chaff fibers and provides fast
computation time compared with other numerical
methods. We use the GEC method to estimate the
RCS of each sub-block and review the GEC method
briefly in this part.

Consider that chaff fibers are randomly distributed
within a rectangular cuboid shaped slab in Fig. 11(a)
and oriented with the orientation distribution $W(\theta, \phi)$.
When a plane wave is normally incident on the tilted
sub-block, the elements of the effective permittivity
matrix of the sub-block for the monostatic RCS
($\hat{k}_i = -\hat{k}_s$) give [23]

$$\varepsilon_{pq} = \varepsilon_0 \left(1 - j \frac{\eta_0}{2\pi} \cdot \rho \lambda^3 \cdot \frac{L}{\lambda} \cdot \bar{\mathbf{I}}_{pq} \right) \qquad (4)$$

where p and q can be either θ or ϕ ($p, q = \theta, \phi$).
The first subscript specifies the polarization of the
scattered wave and the second does the polarization of
the incident field. The symbols η_0, ρ, L, and λ denote
the intrinsic impedance of free space, the average
density of chaff fibers, the length of chaff fibers, and
the wavelength in free space, respectively. $\bar{\mathbf{I}}_{pq}$ is an
effective average current and denotes the weighted
average value of the actual current component $\tilde{\mathbf{I}}_{pq}(\theta, \phi)$
for all directions and is given by

$$\bar{\mathbf{I}}_{pq}(\theta_i, \phi_i) = \frac{\int_\Omega \tilde{\mathbf{I}}_{pq}(\theta, \phi; \theta_i, \phi_i) W(\theta, \phi) d\theta \, d\phi}{\int_\Omega W(\theta, \phi) d\theta \, d\phi} \qquad (5)$$

where $\tilde{\mathbf{I}}_{pq}(\theta, \phi)$ means the current component in the
direction of p-polarization of a single chaff fiber
having a direction of $\hat{l}(\theta, \phi)$ by an incident wave
with q-polarization. θ, θ', and ϕ are the zenith angle,

elevation angle ($= 90°$—zenith angle), and azimuth
angle of the fiber orientation, as shown in Fig. 11(b).
Because the chaff fiber is a straight wire with a cross
section diameter D that is thin compared with the
wavelength ($D \ll \lambda$ and $l \gg D$), there is only an axial
component of current and $\tilde{\mathbf{I}}_{pq}(\theta, \phi)$ is calculated by
the thin-wire approximation of the MoM. $W(\theta, \phi)$ is a
weight function as well as the orientation distribution
of the chaff fiber in air. If the mean μ and standard
deviation σ of the zenith angle θ of chaff fibers are
known, then the orientation distribution $W(\theta, \phi)$ can be
configured as a Gaussian distribution.

$$W(\theta) = \frac{1}{\sqrt{2\pi\sigma^2}} e^{-(\theta-\mu)^2/2\sigma^2}$$
$$W(\phi) = \frac{1}{2\pi} \qquad (6)$$

where $W(\phi)$ is constant since chaff fibers have the
same probability in every direction around the z-axis.

The scattering field from random media such as
a chaff cloud is represented as a sum of the average
field and the fluctuation field. The average field and
fluctuation field are called the coherent field and
incoherent field, respectively [27]. Therefore, the
total RCS from random media is also the sum of the
coherent and incoherent RCS, given as follows [28]:

$$\sigma_{pq} = \sigma_{pq,\text{coh}} + \sigma_{pq,\text{incoh}}. \qquad (7)$$

Obtaining the effective permittivity of the
sub-block yields the coherent and incoherent RCS of
the sub-block. The coherent RCS is obtained by the
boundary problem and the incoherent RCS is obtained
by the RCS of individual chaff fibers [23].

V. SIMULATION RESULTS

The steps of the proposed method are as follows.

1) Set the number and initial conditions (geometry,
orientation, angular velocity, and velocity) of chaff
fibers.

2) Solve 6 DOF equations to calculate the fall
trajectory (position and orientation) of the chaff fibers
as a function of time.

3) Divide the chaff cloud into several sub-blocks
using the octree algorithm.

4) Estimate the orientation distribution (mean and
standard deviation of the orientation) of the chaff
fibers within each sub-block, and construct the weight
function of sub-blocks as the Gaussian distribution.

5) Obtain the effective permittivity of each
sub-block using the incident angle and frequency as
well as the weight function.

6) Calculate the coherent and incoherent RCS
from each sub-block as a homogeneous medium.

7) Obtain the total RCS of the chaff cloud as the
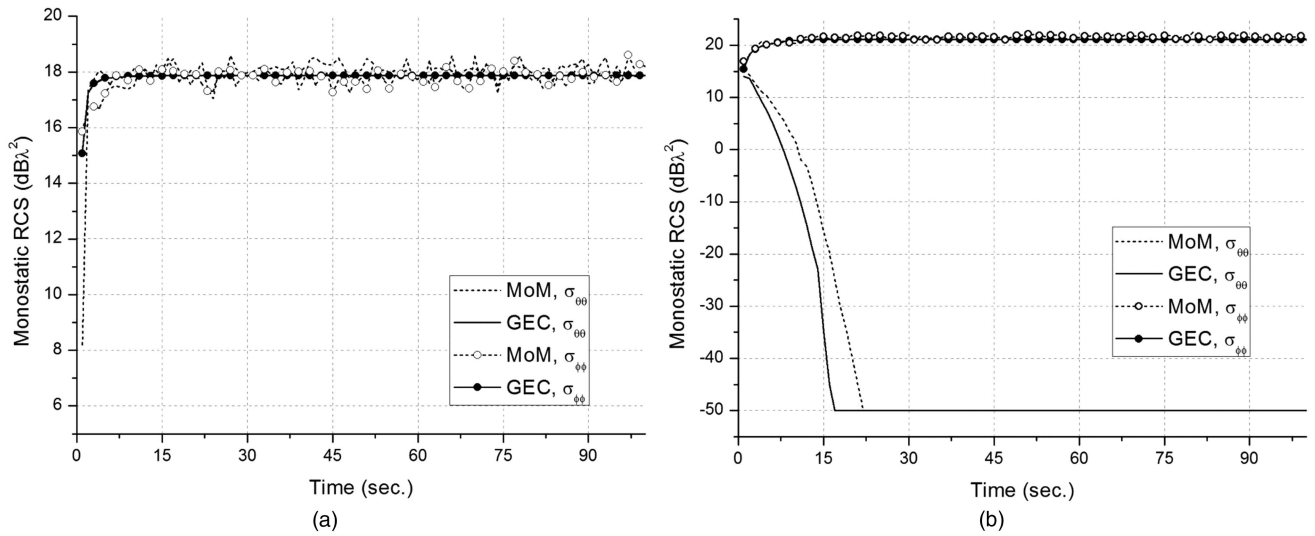sum of the RCSs of all sub-blocks.

Fig. 12. Comparison of monostatic RCS by MoM and GEC method for chaff cloud of one thousand. (a) Straight fibers. (b) Bent fibers.

First, in order to verify the results obtained by the GEC method, we performed a Monte Carlo simulation using the MoM with 360 realizations, as a reference solution. The MoM requires more computer memory and calculation time. Therefore, the number of chaff fibers was set to one thousand which is the maximum number of chaff fibers within a single sub-block. Each chaff fiber is thin and perfectly conducting. The length and aspect ratio (L/D) of all chaff fibers is 1.78 cm and 626, respectively. The initial orientation of the chaff fibers is uniformly random in every direction and the initial angular velocity is 0 m/s. Assume that all chaff fibers begin to fall at the origin ($X = Y = Z = 0$ m) and there is no influence of wind.

Figure 12 shows the monostatic RCSs of one thousand straight fibers and bent fibers normalized to λ_0^2, in resonance frequency, when the incident plane wave illuminates the origin of the chaff cloud at $\theta_i = 90°$. For one thousand straight fibers, the disparity between the results of the two methods is roughly 0.5 dB. However, the results obtained by the GEC method are in good agreement with those obtained by MoM. On the other hand, for bent fibers, the two methods give the $\phi\phi$-polarization RCSs in satisfactorily close agreement, but there exists about a 5–10 dB difference between the $\theta\theta$-polarization RCSs of the two methods in the section of $t = 1$–20 s. This inaccuracy is attributed to the value of the RCS drastically falling. Nevertheless, the pattern of the two results is similar. The effect of polarization and the type of chaff fibers, as well as the variance of the RCS over time, are discussed later.

In order to estimate the RCS of an actual chaff cloud, the numbers of chaff fibers is set to ten thousand and one million, respectively. We estimate the aerodynamics characteristic of falling bent fibers with 1 s interval from 1 s to 100 s, and then calculate the RCS of straight fibers as a function of time. The geometry of the chaff fibers and the initial conditions are identical to the previous case. Figure 13(a) shows the monostatic RCS of a chaff cloud consisting of straight fibers versus falling time when the incident field illuminates the chaff cloud at $\theta_i = 90°$.

In the case of ten thousand chaff fibers, the monostatic RCS has a minimum value at the most densely placed time, $t = 0$ s. The RCS increase with the elapse of time. After about 10 s, the RCS is constant at about 28 dBλ^2. In the case of one million chaff fibers, after the chaff fibers fall, the RCS begins to increase dramatically and has overshoot at $t = 8$ s. After overshoot, the RCS gradually increases and reaches the steady state. From Fig. 13(b), it is seen that the average scatterer spacing of ten thousand chaff fibers increases more rapidly than the case of one million fibers as time passes. This is a result of the RCS of ten thousand chaff fibers reaching the steady state more rapidly than for the case of one million chaff fibers. It is known that the coupling effect can be negligible when the average scatterer spacing is larger than 2.0λ [29]. That is, if the spacing between adjacent fibers is larger than 2λ, then the RCS is in direct proportion to the number of chaff fibers and has constant value of the steady state. The average scatterer spacing of one million chaff fibers is still smaller than 2.0λ at $t = 40$ s. Therefore, the RCS does not reach the steady state and slowly increases. It can then be expected that the RCS in the steady state is 48 dBλ^2, which is 20 dB greater than that of ten thousand chaff fibers, because the number of chaff fibers is 100 times (20 dB) more than ten thousand chaff fibers. Meanwhile, the results of $\theta\theta$-polarization and $\phi\phi$-polarization appear to be overlapped, since the orientation of straight fibers has the same probability
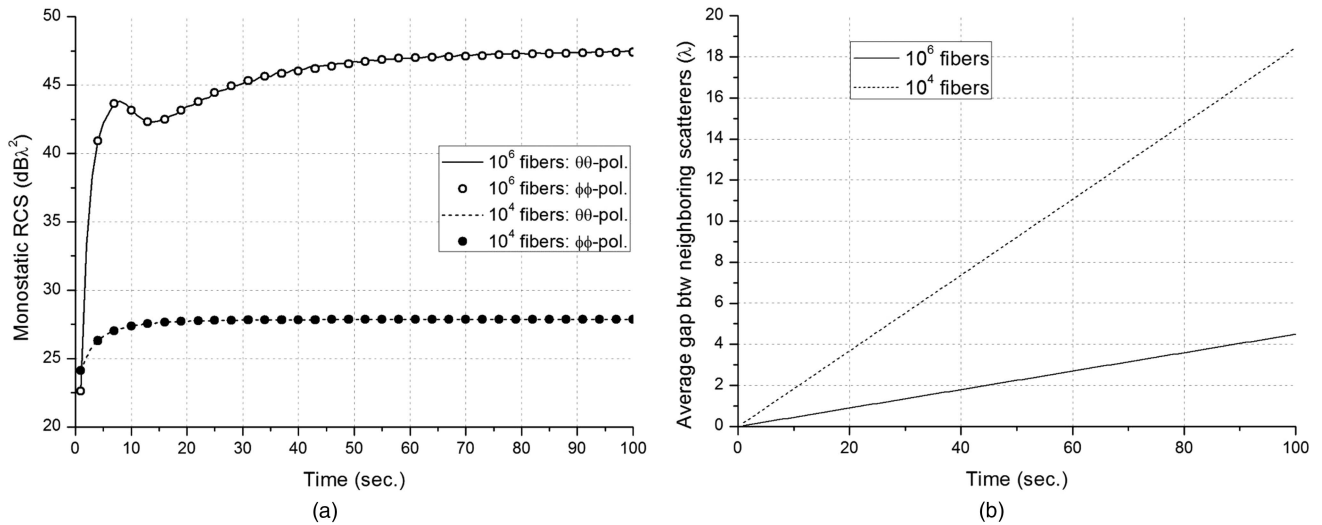
SEO, ET AL.: DYNAMIC RCS ESTIMATION OF CHAFF CLOUDS

2123

Fig. 13. Simulated results for 10^6 and 10^4 straight fibers at $\theta_i = 90°$. (a) Monostatic RCS of chaff cloud as function of time. (b) Average gap between neighboring scatterers.
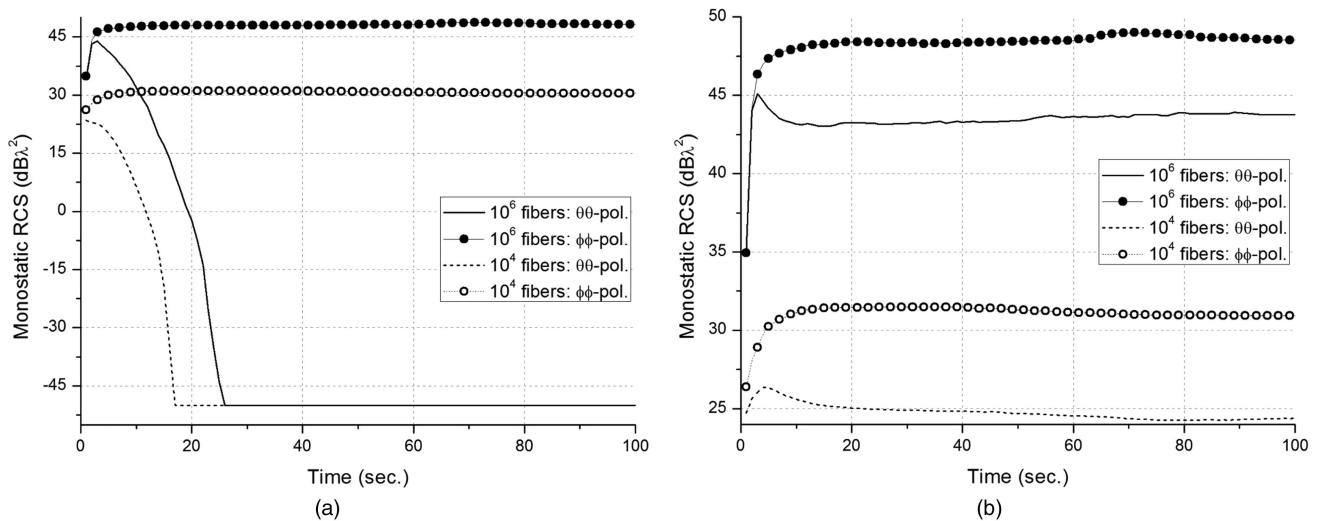

Fig. 14. Monostatic RCS of 10^6 and 10^4 bent fibers as function of time. (a) At $\theta_i = 90°$ (b) At $\theta_i = 135°$.

in every direction and is constantly maintained during free flight, as previously stated in Section III.

Unlike straight fibers, bent fibers are horizontally oriented during free flight in the air. To explore the effect of this characteristic of bent fibers, the longitudinal bend (R/L) of bent fibers is randomly selected in a range of 1 to 100. The remaining initial conditions are identical to the previous case of straight fibers. Figure 14 shows the RCS as a function of time for ten thousand and one million bent fibers.

For a plane wave with $\theta_i = 90°$, the $\phi\phi$-polarization RCSs are illustrated by circular symbols in Fig. 14(a). Directly after the descent of chaff fibers, the $\phi\phi$-polarization RCSs of ten thousand and one million chaff fibers have small values as a result of conglomerated fibers. But the $\phi\phi$-polarization RCSs increase sharply as time passes. The RCS of ten thousand bent fibers has a constant level of 30.5 dBλ^2 after about 10 s, while the RCS of one million bent

fibers has almost a constant level of 47 dBλ^2. It appears that the RCSs of ten thousand and one million fibers reach the steady state level with the passage of time. In the steady state, however, the RCS of one million bent fibers is not 20 dB greater than that of ten thousand bent fibers. This is because the shape of the chaff cloud of the bent fibers changes very little after approximately 20 s, as shown in Fig. 6(a). That is, in the steady state, the spacing between adjacent fibers is smaller than 2λ and is maintained, unlike the case of straight fibers. On the other hand, the $\theta\theta$-polarization RCS pattern is completely different from the $\phi\phi$-polarization RCS pattern. For the case of ten thousand bent fibers, the $\theta\theta$-polarization RCS continuously decreases from the outset and falls below -50 dBλ^2 after 20 s. In contrast, for the case of one million bent fibers, the $\theta\theta$-polarization and $\phi\phi$-polarization RCS resemble each other in the initial stage. However, chaff fibers began to orient

IEEE TRANSACTIONS ON AEROSPACE AND ELECTRONIC SYSTEMS VOL. 48, NO. 3 JULY 2012
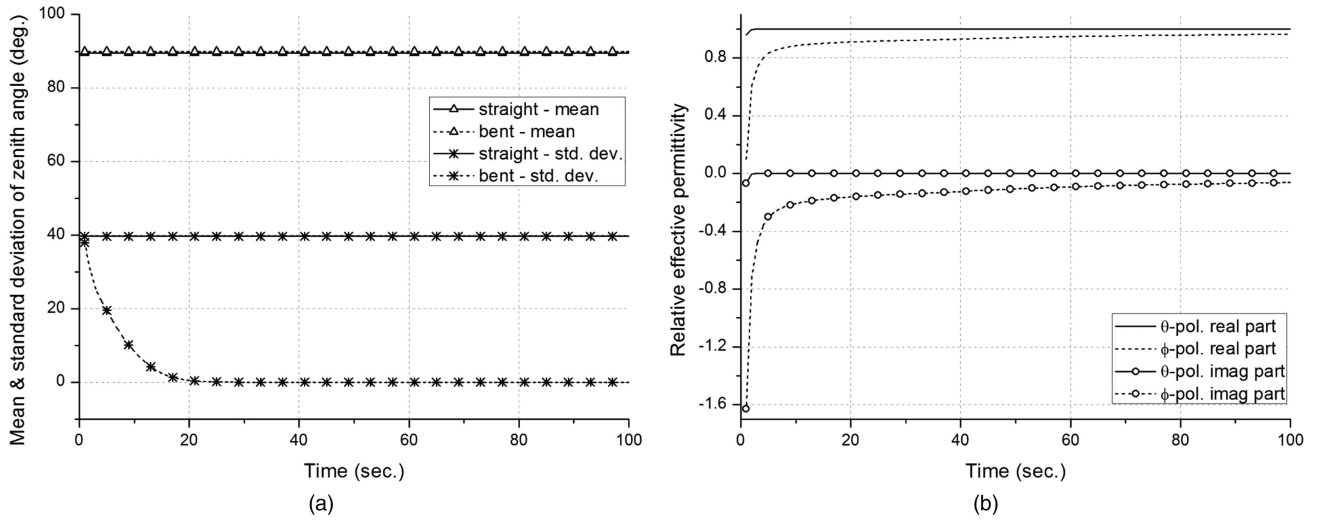
Fig. 15. (a) Mean and standard deviation of zenith angle for straight fibers and bent fibers. (b) Relative effective permittivity of chaff cloud for ten thousand bent fibers at $\theta_i = 90°$.

horizontally and then the $\theta\theta$-polarization RCS rapidly decreased. Meanwhile, the $\theta\theta$-polarization RCS appears to converge at -50 dBλ^2 as time passes, because the values of less than -50 dBλ^2, influenced by the numerical precision of the computer, are set to -50 dBλ^2.

The unique characteristics of the $\theta\theta$-polarization RCS can be explained by the zenith angle of the fiber orientation and the effective permittivity. As shown in Fig. 15(a), the mean and standard deviation of the zenith angle of straight fibers have constant values during the falling time, while the standard deviation varies from $40°$ to $0°$ for the bent fiber. A standard deviation in the vicinity of $0°$ indicates that almost all fibers have a zenith angle of $90°$ and horizontal orientation. Thus, the bent fibers do not have a θ-component. As shown in Fig. 15(b), the variation of orientation of fibers has different effects on the effective permittivity under different polarizations. Bent fibers having a horizontal orientation are not affected by a θ-polarized field but rather by a ϕ-polarized field as time passes. Therefore, the effective permittivity by the θ-polarized field converges to the permittivity of air, $\varepsilon_{\theta\theta} \approx \varepsilon_0(1 - j0)$, and then the $\theta\theta$-polarization RCS has a very small value, but the $\phi\phi$-polarization RCS has a large value.

Fig. 14(b) shows the average RCS of the chaff cloud under the same conditions as in the case of Fig. 14(a) when a plane wave is incident on the chaff cloud at $\theta_i = 135°$. The $\phi\phi$-polarization RCS at an incident angle $\theta_i = 135°$ is similar to that at an incident angle $\theta_i = 90°$, but the $\theta\theta$-polarization RCS has a considerable difference. The $\theta\theta$-polarization RCS at an incident angle $\theta_i = 90°$ is approximately 0 (-50 dBλ^2) for the most part, while the $\theta\theta$-polarization RCS of ten thousand and one million chaff fibers is about 25 dBλ^2 and 44 dBλ^2, respectively, at an incident angle

$\theta_i = 135°$. The unit vector of the θ-direction is $\hat{\theta} = \hat{x}\cos\phi_i\cos\theta_i + \hat{y}\sin\phi_i\cos\theta_i - \hat{z}\sin\theta_i$ and a function of the incident angles θ_i and ϕ_i. Since the unit vector of the θ-direction at an incident angle $\theta_i = 90°$ only has a z-component, the θ-polarized field is not affected by chaff fibers having a horizontal orientation. However, the θ-polarized field at $\theta_i = 135°$ is affected by the x- and y-components of chaff fibers having a horizontal orientation, and the $\theta\theta$-polarization RCS at $\theta_i = 135°$ is larger than that at $\theta_i = 90°$. We observed that the scatterers to be aligned along one direction as time elapses are significantly affected by the incident angle.

VI. CONCLUSION

This paper has described a procedure for simulating the trajectory of chaff fibers and a method of calculating the RCS for chaff clouds. In order to simulate the actual situation of falling chaff fibers, we predicted the aerodynamics of one million straight fibers and bent fibers in the air. Information about the chaff cloud as a function of time consists of the position and orientation of each chaff fiber, obtained from of the aerodynamics. The chaff cloud was divided into sub-blocks by an octree algorithm. The GEC method was applied to calculate the RCS of each sub-block. This calculation was repeated every second and the total RCS of the chaff cloud was predicted as a function of time.

The results shown here are the RCS of a chaff cloud with one type of chaff fiber at the resonant frequency, but the response to different frequencies can also be calculated. In addition, because the frequency response can be calculated by the GEC method, the RCS of a chaff cloud consisting of chaff fibers of various lengths can be calculated. These calculations and procedure can be used to design chaff and to deceive guided weapons effectively. The

calculation process used in this paper can be applied to chaff not only with a fiber shape but also various other shapes.

REFERENCES

[1] Sucker, D. and Brauer, H.
Fluiddynamik bei der angestromten Zylinder.
Wärme und Stoffübertragung, **8** (1975), 149–158.

[2] Curle, S. N.
Calculation of the axisymmetric boundary layer on a long thin cylinder.
In *Proceedings of the Royal Society of London, Series A, Mathematical and Physical Sciences*, **372** (Oct. 1980), 555–564.

[3] Brunk, J., Mihora, D., and Jaffe, P.
Chaff aerodynamics.
Report AFAL-TR-75-81, 1975.

[4] Wilkin, J. H.
The measurement of dipole angle distribution.
Report DAJA-81-C-0182, 1982.

[5] Palermo, C. J. and Bauer, L. H.
Bistatic scattering cross section of chaff dipoles with application to communications.
Proceedings of the IEEE, **53** (Aug. 1965), 1119–1121.

[6] Arnott, W. P., et al.
Determination of radar decoy diameter distribution function, fall speed, and concentration in the atmosphere by use of the NEXRAD radar.
Desert Research Institute, Reno, NV, 2004. Available: http://www.patarnott.com/pdf/decoyRadarandFallSpeed.pdf.

[7] Butters, B. C. F.
Chaff.
IEE Proceedings—Pt. F, **129**, 3 (June 1982).

[8] Wu-Xianli, et al.
Chaff jamming effect to radar and math model building.
In *Proceedings of the International Conference on Radar (CIE)*, 2006, pp. 1–5.

[9] Jian-chun, M., et al.
Math model building and echo simulation of chaff clouds jamming.
In *2009 IET International Radar Conference*, Guillin, China, Apr. 2009, pp. 1–4.

[10] Della Ducata, D., et al.
A comprehensive model for chaff characterization.
In *Proceedings of the European Radar Conference*, Rome, 2009, pp. 485–488.

[11] Qu, C. and Li, Y.
Research on airborne chaff centroid jamming to ground radar.
In *Proceedings of the 2010 IEEE 10th International Conference on Signal Processing*, Beijing, 2010, pp. 2250–2252.

[12] Wu, X., et al.
Research on applications of chaff.
In *Proceedings of the 2006 8th International Conference on Signal Processing*, vol. 4, Beijing, 2006.

[13] Marcus, S. W.
Dynamics and radar cross section density of chaff clouds.
IEEE Transactions on Aerospace and Electronic Systems, **40**, 1 (Jan. 2004).

[14] Burke, G. J.
Numerical electromagnetics code (NEC)-Method of Moments; Part I: Program description—Theory, Part II: Program description—Code, Part III: User's guide.
Lawrence Livermore National Lab., Report UCID-18834, Jan. 1981.

[15] Taflove, A. and Haqness, S. C.
Computational Electrodynamics: The Finite-Difference Time-Domain Method (3rd ed.).
Norwood, MA: Artech House, 2005.

[16] Sevgi, L.
Complex Electromagnetic Problems and Numerical Simulation Approaches.
Hoboken, NJ: Wiley-IEEE Press, 2003.

[17] Tai, C-T.
Electromagnetic back-scattering from cylindrical wires.
Journal of Applied Physics, **23** (1952), 909–916.

[18] Cassedy, E. and Fainberg, J.
Back scattering cross sections of cylindrical wires of finite conductivity.
IRE Transactions on Antennas and Propagation, **8**, 1 (1960), 1–7.

[19] Richards, M. A., et al.
A model radar cross section of thin-wire targets via the singularity expansion method.
IEEE Transactions on Antennas and Propagation, **40**, 10 (Oct. 1992).

[20] Perotoni, M., et al.
3D electromagnetic evaluation of a chaff cloud.
Microwave Journal, **53**, 8 (2010).

[21] Macedo, A. D. F.
Analysis of chaff cloud RCS applying fuzzy calculus.
In *Proceedings of the 1997 SBMO/IEEE MTT-S International Microwave and Optoelectronics Conference*, vol. 2, 1997, pp. 724–728.

[22] Pouliguen, P., et al.
Simulation of chaff cloud radar cross section.
In *2005 IEEE Antennas and Propagation Society International Symposium*, vol. 3A, July 2005, pp. 80–83.

[23] Seo, D-W., et al.
Generalized equivalent conductor method for a chaff cloud with an arbitrary orientation distribution.
Progress in Electromagnetics Research, **15** (2010), 336–346.

[24] Turner, J. W. and Charles, Jr., H. F.
Countermeasure radar chaff.
U.S. Patent 3,544,997, Dec. 1, 1970.

[25] Nelson, R. C.
Flight Stability and Automatic Control.
New York: McGraw-Hill, 1997.

[26] Press, W. H., et al.
Runge-Kutta method.
In *Numerical Recipes in FORTRAN* (2nd ed.), New York: Cambridge University Press, 1992, pp. 704–708.

[27] Ishimaru, A.
Wave Propagation and Scattering in Random Media.
Hoboken, NJ: Wiley-IEEE Press, 1994.

[28] Marcus, S. W.
Electromagnetic wave propagation through chaff clouds.
IEEE Transactions on Antennas and Propagation, **55** (July 2007), 2032–2042.

[29] Wickliff, R. G. and Garbacz, R. J.
The average backscattering cross section of clouds of randomized resonant dipoles.
IEEE Transactions on Antennas and Propagation, **22**, 3 (May 1974), 503–505.

Dong-Wook Seo was born in Ulsan, Korea, on November 28, 1980. He received the B.S. degree in electrical engineering from the Kyung Pook National University, Daegu, Korea, in 2003, and the M.S. and Ph.D. degrees in electrical engineering from the Korea Advanced Institute of Science and Technology (KAIST), Daejon, Korea, in 2005 and 2011, respectively.

Since 2011, he has been a senior researcher with the Defense Agency for Technology and Quality (DTaQ), Daegu, Korea. His work is focused on the development and production of electronic warfare systems. His current research interests include numerical techniques in the area of electromagnetics, electronic warfare system, and wireless channel modeling.

Hyun-jae Nam received the B.S. and M.S. degrees in aerospace engineering from the Korea Advanced Institute of Science and Technology (KAIST), Daejon, Korea, in 2007 and 2009, respectively.

Currently, he is a Ph.D. candidate in the Department of Aerospace Engineering at KAIST. His recent research interests include electromagnetic radiation, rarified gas dynamics, hypersonic aerothermodynamics, and nozzle flow analysis.

Oh-Joon Kwon was born in Andong, Korea, in 1956. He received the B.S. degree in aeronautical engineering from Seoul National University, Korea, in 1979, the M.S. degree from the Korea Advanced Institute of Science and Technology (KAIST) in 1981, and the Ph.D. degree in aerospace engineering from the Georgia Institute of Technology, Atlanta, GA, in 1988.

He was a research engineer at the Korea Institute of Aeronautical Technology, Seoul, Korea, from 1981 to 1984, and worked as a research associate at the Georgia Institute of Technology from 1989 to 1991. He also worked as a research engineer at the NASA Lewis Research Center, Cleveland, OH, from 1991 to 1994. He joined the Korea Advanced Institute of Science and Technology (KAIST) in 1994, and is currently a professor in the Department of Aerospace Engineering at KAIST. His research interests include computational aerodynamics, rotorcraft aerodynamics and aeroelasticity, turbomachinery flow analysis, unsteady aerodynamics, parallel computing, and rarefied gas flows.

Noh-Hoon Myung was born in Seoul, Korea, in 1953. He received the B.S. degree in electrical engineering from Seoul National University, Korea, in 1976, and the M.S. and Ph.D. degrees from The Ohio State University, Columbus, in 1982 and 1986, respectively.

For six years, he was a research member at the ElectroScience Laboratory, Ohio State University, working in the area of electromagnetic wave scattering and propagation. He joined the Korea Advanced Institute of Science and Technology (KAIST) in 1986, where he is currently professor at the Department of Electrical Engineering in the emerging device group as well as Director of the Satellite Technology Research Center (SaTReC), Daejeon, Korea. His current research areas include wave scattering and propagation analysis, radar cross-section analysis, antenna and radar system design, mobile and satellite communications, and electromagnetic interference and electromagnetic compatibility.